

# Fluorescence Study of Film Formation From Hard/ Soft Latex Blends

Şaziye UĞUR,1\* Yves HOLL2

<sup>1</sup>Istanbul Technical University, Department of Physics, 34469 Maslak, Istanbul-Turkey

Fax:+90(212)2856386; e-mail:saziye@itu.edu.tr

<sup>2</sup> University Louis Pasteur and Institute Charles Sadron (CNRS) 6, rue Boussingault BP

40016 67083 Strasbourg Cedex-France

Fax: +333 90 24 49 64; e-mail:holl@ics.u-strasbg.fr

(Received: 8 May, 2006; published: 14 July, 2006)

Abstract: The effects of blend composition on film formation is studied using the SSF and UV-visible (UVV) techniques. Latex blend films were prepared from mixtures of two types of particles in dispersion, one composed of a high-T<sub>q</sub> (hard) pyrene (P) labeled polystyrene (PS) latex; the other a low-T<sub>g</sub> (soft) poly(n-butyl acrylate) (BuA1). Twelve different blend films were prepared in various hard/soft latex compositions at room temperature and annealed at elevated temperatures above glass transition temperature (T<sub>g</sub>) of polystyerene for 10 min. Fluorescence intensity (I<sub>P</sub>) from P was measured after each annealing step to monitor the stages of film formation. The evolution of transparency of latex films was monitored using photon transmission intensity, Itr. Film morphologies were examined by atomic force microscopy (AFM). The results showed that as the amount of hard component in the blend is decreased, a significant change occured in both I<sub>P</sub> and I<sub>tr</sub> curves at a certain critical weight fraction (50%wt) of PS hard latex. Above this fraction two distinct film formation stages, which are named as void closure and interdiffusion were seen in fluorescence data. However, below 50%wt PS no film formation stages were observed. Below this fraction, I<sub>tr</sub> data showed that phase separation process occurs between PS and BuA1 polymers. These results were also confirmed by AFM pictures. Film formation stages for 50-100%wt range of PS were modeled and related activation energies were calculated. There was no observable change in activation energies confirming that film formation behavior is not affected by varying the blend composition.

#### Introduction

The latex film formation process has been extensively studied for latex systems containing a single polymer compositions [1-11]. Film formation from low- $T_g$  (soft) and high- $T_g$  (hard) latex dispersions can occur in several stages [1,2]. In both cases, the first stage corresponds to the wet initial stage. Evaporation of solvent leads to second stage in which the particles form a close packed array, here if the particles are soft they are deformed to polyhedrons. Hard latex however stays undeformed at this stage. Annealing of soft particles causes diffusion across particle-particle boundaries which leads to a homogeneous continuous material. In the annealing of hard latex system, however, deformation of particles first leads to void closure [12-14] and then after the voids disappear diffusion across particle-particle boundaries starts,

i. e. the mechanical properties of hard latex films evolve during annealing; after all solvent has evaporated and all voids have disappeared. The last stage of film formation is the coalescence of the particles where macromolecules belonging to different particles mix by interdiffusion [15,16].

Dry films of such polymers have poor mechanical properties. Polymer with low-T<sub>g</sub> are eaisly deformed and yield excellent film formation properties. However, the film produced will often be tacky, have poor mechanical properties and solvent resistance. High-T<sub>g</sub> polymers yield particles that do not deform easily, and they require solvents as plasticizers to help the film formation. In order to get films with good mechanical and barrier properties, composite latex systems involving two or more different polymer compositions can be used [17-19]. One approach to do this is the synthesis of waterborne core/shell latex particles with a high-T<sub>g</sub> polymer core and a film-forming shell. Another technique is by physically blending two polymer latexes with different T<sub>q</sub> values [20,21] in which the soft latex will form a film and become the continuous phase while the hard particles will act as filler and impart mechanical properties [17,22]. A blend of low  $T_g$  latex with a high- $T_g$  polymer is used in latexbased impact modifiers for polymer resins [23], in automotive and architectural coatings, membranes, etc. One of the main interests in latex blends is the drive towards zero-volatile organic compounds in the organic coating industry[24]. blend one can obtain different properties than those of the individual components, and under some circumstances might even obtain unique properties[25].

Several research groups have recently studied polymer blends of hard and soft latices [19-21,26,27]. Feng and Winnik [20] have demonstrated that a film forming soft latex can be blended with a non-film forming hard latex to produce a film in which the continuous phase is comprised of the soft latex. They revealed that aggregates of hard particles produce turbidity in the blend films [20]. They later reported that the addition of hard particles in latex blends greately improves mechanical performance of acrylic latices [17]. Environmental-SEM [21] has revealed that clusters of hard acrylic particles create air voids in blends with a soft film forming acrylic latex. Over long periods of time these voids shrink in size as the soft latex flows and fills the voids space. Theories of sintering adequately describe the process [21]. This sintering process is slowed down as the concentration of non-film forming particles increases. Analysis of morphology and transparency of latex blend films by atomic force microscopy (AFM) and scanning electron microscopy (SEM) has provided insight into the interaction between hard and soft latex particles [20,28]. Although diffusion at the particle/particle interface of miscible polymer components during film formation is studied extensively [7-10,29,30] little is known about the diffusion of polymer across the interface between immiscible and partially miscible polymers in latex blends. The limited interdiffusion near the phase separation temperature of the latter is thermodynamically controlled. Although the film microstructure of latex blends is closely related to void formation and the mechanical, optical and barrier properties [20,24], the evolution of mechanical properties of latex films depends on polymer diffusion across the latex particle interface [31,32].

In the present work, we have studied the film formation behavior of the hard (PS)/soft (BuA1) latex blends depending on blend composition by means of fluorescence and UVV techniques. Different compositions of blend were prepared and annealed above the glass transition temperature of PS ranging from 90 to 250  $^{\circ}$ C for 10 min. The evolution of film formation from PS/BuA1 blend was studied by monitoring pyrene emission intensity,  $I_P$  from pyrene labeled PS and transmitted photon intensity,  $I_{tr}$  in

blend films. The surface morphologies were examined with atomic force microscopy (AFM). The results showed that at 50-100%wt range of PS two distinct film formation stages named as void closure and interdiffusion processes take place upon annealing. In this range of PS, it was found that extensive coalescence of PS particles occured and coalesced PS domains provides a continous film. However, below 50%wt PS content the coalescence of PS domains was prevented by soft BuA1 matrix and no film formation stages were seen. The UV data showed that PS and BuA1 undergo phase separation below this fraction.

## **Results and discussion**

Fluorescence emission spectra of 80 and 30 wt% PS content blend films annealed at various temperatures for 10 min are shown in Figure 1a and b, respectively.

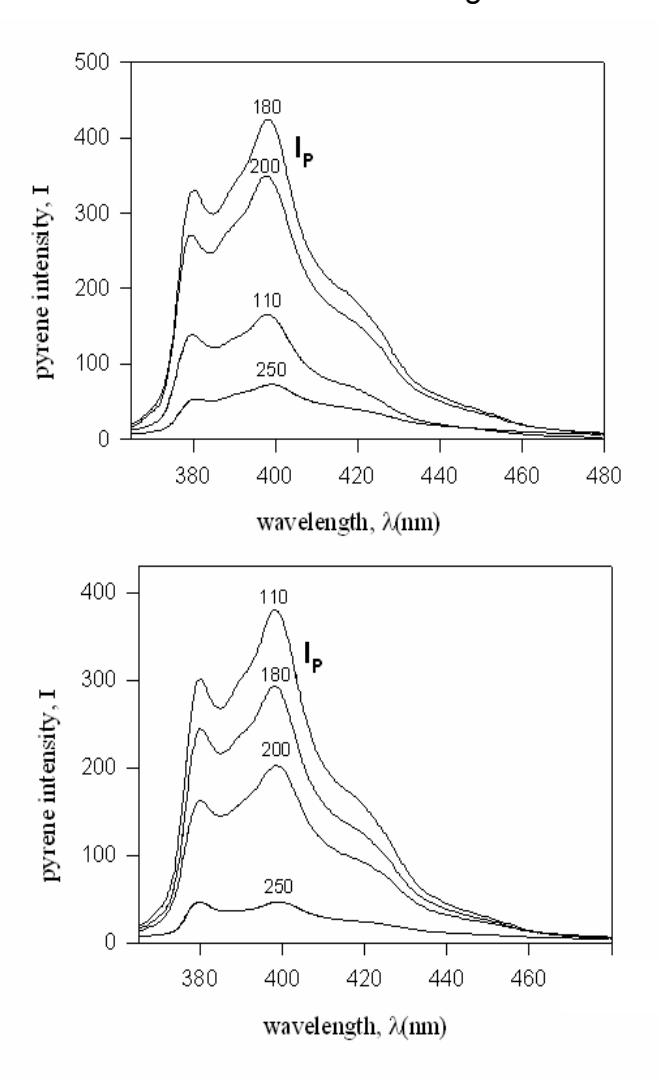


**Fig. 1.** Fluorescence emission spectra from **a-** 80 and **b-** 30 wt% PS content blend films annealed in 10 min time intervals. Numbers on each curve present the annealing temperature.

As the annealing temperature is increased, fluorescence intensity, I<sub>P</sub> from the blend film with 80 wt% PS first increased and then decreased with increasing annealing temperatures. However, for the 30 wt% PS content blend film, I<sub>P</sub> intensity decreased.

The plot of  $I_P$  versus annealing temperature, T for 100, 80, 50, 30, 20 and 10 wt% PS content blend films are shown in Fig. 2.

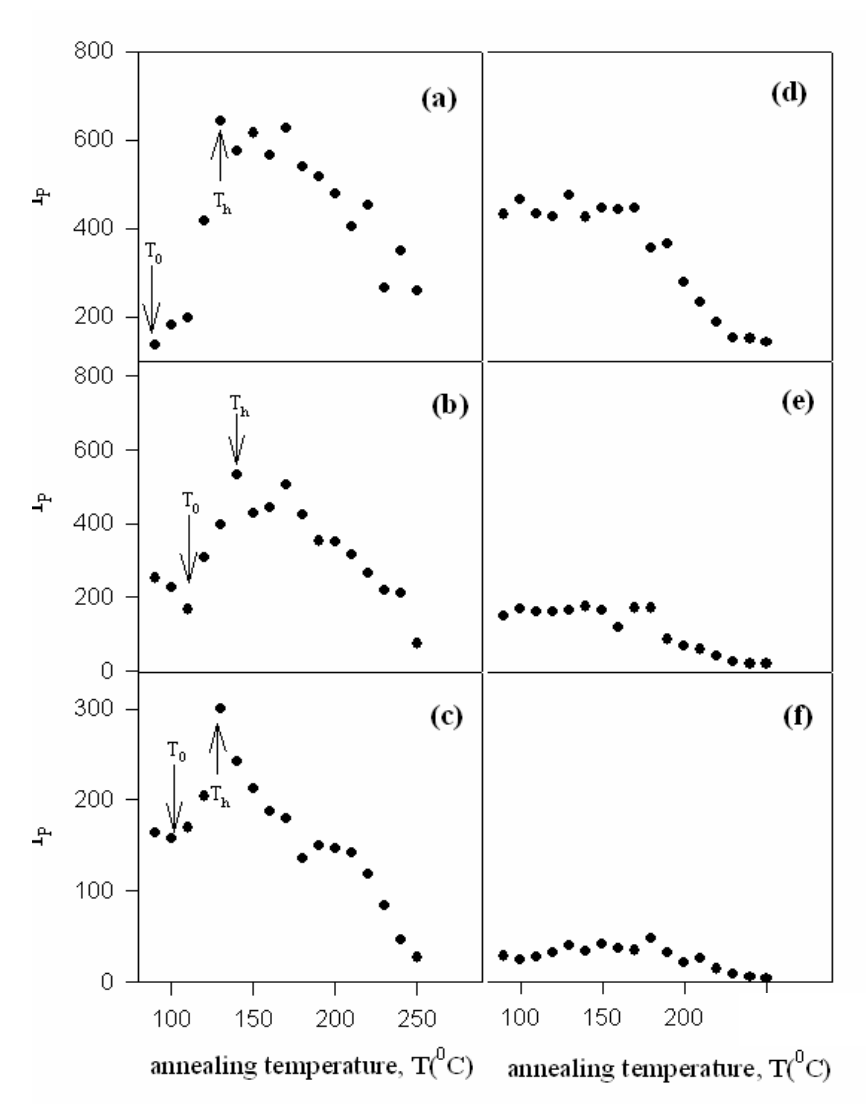
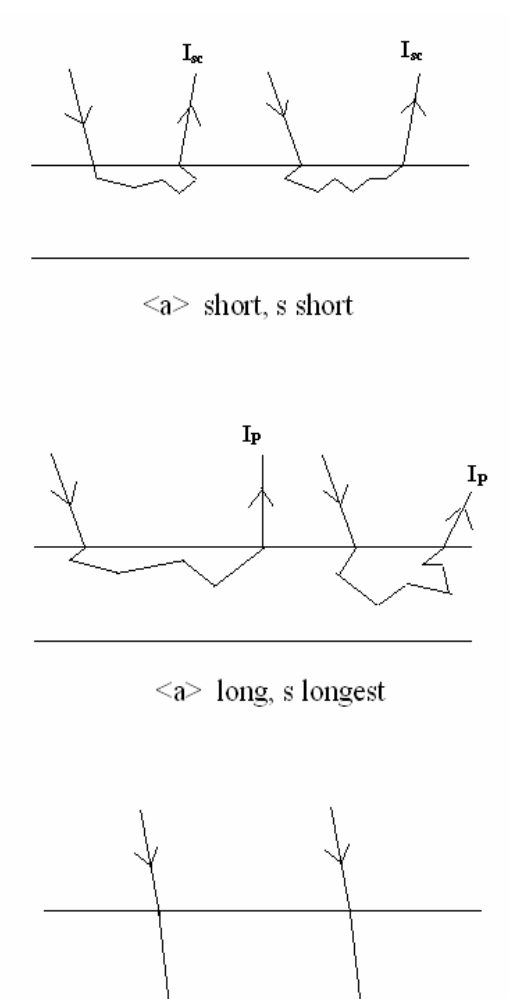


**Fig. 2.** Plot of fluorescence intensities,  $I_P$  versus annealing temperature, T for the blend films contain **a-** 100, **b-** 80, **c-** 50, **d-** 30, **e-** 20 and **f-** 10 wt%PS latex.  $T_0$  and  $T_h$  are the minimum film formation and healing temperatures, respectively.

It is seen that  $I_P$  intensity from blends with 100, 80 and 50 wt% PS content increases upon annealing above a certain temperature called minimum film formation temperature,  $T_0$ . Then, due to the further annealing,  $I_P$  decreases by showing a maximum at certain temperature called as healing temperature,  $T_h$ . The increase and decrease of  $I_P$  upon annealing of these blend films can be explained with the void closure and interdiffusion processes, respectively [9,10]. However,  $I_P$  intensity from blends which have 30, 20 and 10 wt% PS behave quite differently (Figure 2d-f). In other words,  $I_P$  intensities from the blends prepared with low PS content are weak and almost remains unchanged during annealing incidating that no film formation process takes place.



 $I_{tr}$ 

**Fig. 3.** Schematic illustration of change in pyrene intensity ( $I_P$ ) related with variation in mean free and optical paths (<a> and s) during film formation from (50-100)%wt PS content blend film; **(a)** before annealing, **(b)** film after void closure process is ended, **(c)** transparent film.

<a> longest, s short

 $I_{tr}$ 

The behavior of  $I_P$  in blend films for the 50-100%wt range of PS during annealing is schematically presented in Fig 3a-c, respectively. The variation in  $I_P$  depends on optical path, s, of a photon in the blend [9,10]. This optical path is directly proportional to the probability of a photon encountering a pyrene molecule. In Fig 3a, since the film posses many voids the photon is scattered from the particle surface which results in short mean-free (<a>) and optical path (s) yielding very low  $I_P$ . Figure 3b shows a film in which interparticle voids disappear due to annealing giving rise to a long mean free (<a>) and optical path, s in the film. Clearly, in this regime, with the same number of re-scatterings, a photon will spend some time in the blend, and consequently,  $I_P$  values are large. Due to the further annealing (Fig 3c) the blend starts to become essentially transparent to the photon, the mean free path diverges, and s eventually becomes short i.e of the order of the blend thickness, d. Hence, the decrease in  $I_P$  after complete annealing has occured.

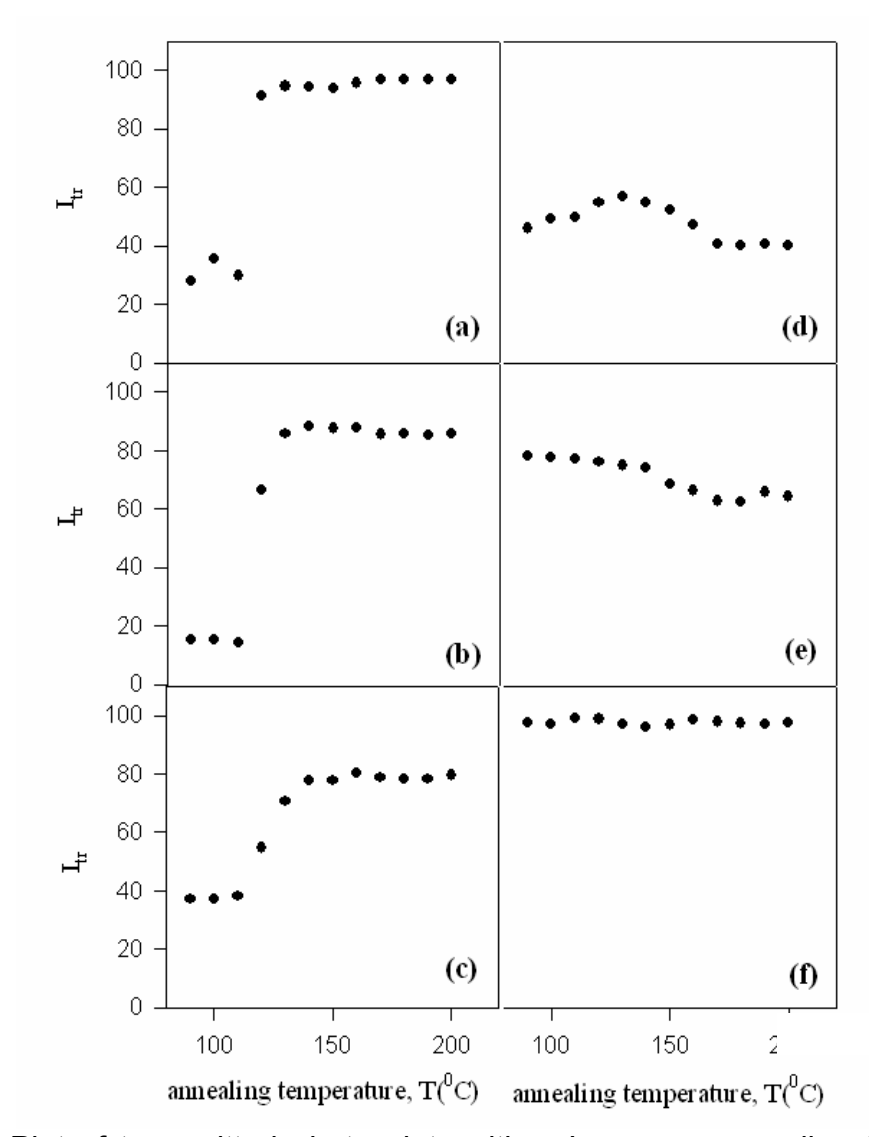


**Fig. 4.** Plot of transmitted photon intensities, I<sub>tr</sub> versus annealing temperatures, T from the blend films contain **a-** 100, **b-** 80, **c-** 50, **d-**30, **e-** 10 and **f-** 0 wt%PS latex.

The change in transmittance of the blend films upon annealing are shown in Fig 4 with decreasing (100, 80, 50, 30, 10 and 0 wt%) PS component. It is seen in Fig 4a, b and c that, It present a dramatic increase above the minimum film formation temperature, T<sub>0</sub> as similar to the fluorescence result. It increases reaching a maximum and then remains constant for 100, 80 and 50 wt%PS content blend film with annealing. The increasing of It with annealing temperature primarily due to the closure of voids [8-10] between PS particles by viscous flow in these films. However, it is seen in Fig 4(d-f) that for 30, 20 and 10 wt% PS composition It almost doesn't change with annealing temperature. It means that these curves present no void closure phenomenon in consistent with the fluorescence results. Although transparency of these films almost does not change with increasing temperature, Itr shows a sudden decrease at 30%wt PS. Then it starts to increase for 10%wt PS and becomes maximum again for 0%wt PS (pure BuA1 film). Since the PS and BuA1 are indeed immiscible polymers, the decrease in It can be explained with the phase separation process between two polymers during coalescence of PS latexes. Here, it has to be noted that pure BuA1 film is optically clear at all annealing temperature, because coalescence of the soft particles occurs at room temperature with the

evaporation of the water without thermal ageing. On the other hand, optical clarity of pure PS film increases with annealing temperature and reaches the same optical clarity with the pure BuA1 film corresponding to void-free and fully-dense film at the end of the annealing process.

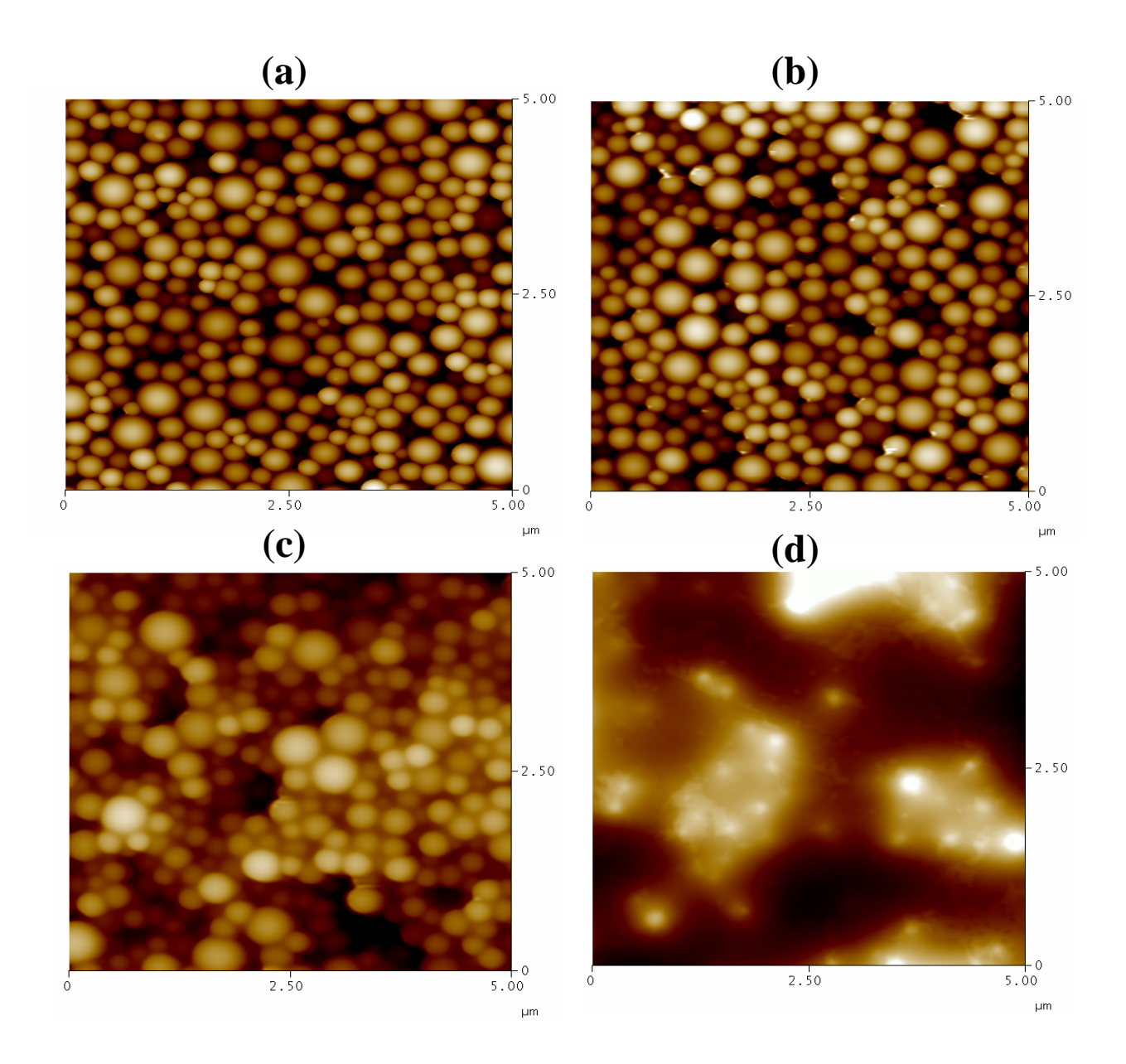


**Fig. 5.** AFM images of blend film prepared with **a-** 100, **b-** 80, **c-** 50 and **d-** 30 wt%PS latex annealed at 110  $^{\circ}$ C.

In Figs 5-8, we present AFM images of the blends which have 100, 80, 50 and 30 wt% contents of PS at different annealing temperatures. At 110  $^{0}$ C (Fig 5), no deformation in PS particles is observed. In Fig 5a and b, for the films containing 100 and 80 wt% PS particles, the hard spheres seem to be randomly distributed and contain a lot of voids which give highly opaque film. However, AFM images in Fig 5c and d show that the soft particles undergo complete coalescence and fill the voids between the hard particles with covering them. There is tendency for the hard

particles to aggregate in these films. In Fig 5d for 30 wt% PS content film, hard particles are completely imbedded in the continous phase generated by the soft latex and small PS aggregates are clearly apparent which cause the turbidity in the blend. Here light and dark areas correspond to high and low regions in the film. With annealing the films at  $130\,^{\circ}$ C, the high density of contacts between PS particles takes place due to the void closure and induces the extensive PS aggregation (Fig 6a, b and c).

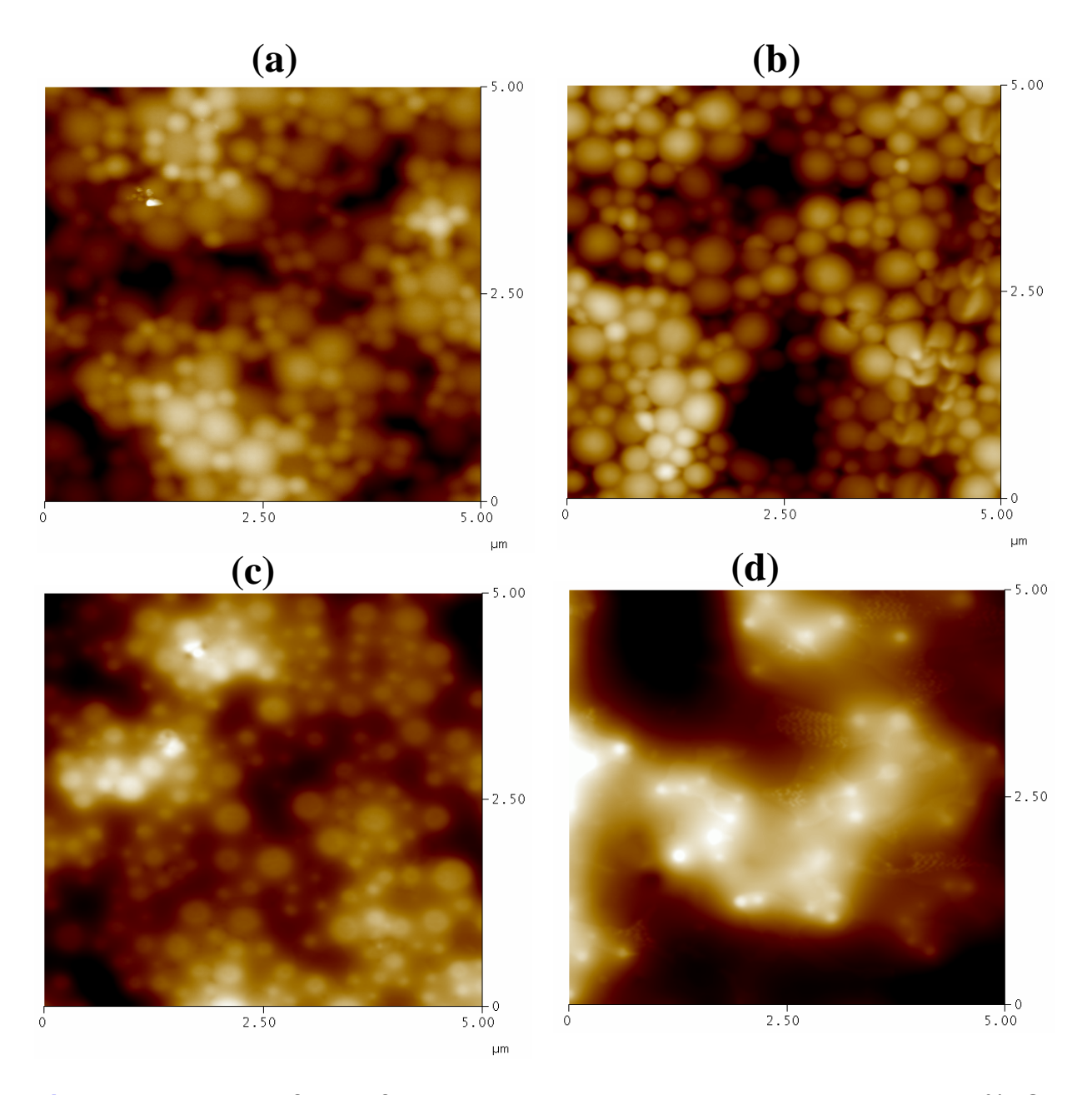


**Fig. 6.** AFM images of blend film prepared with **a-** 100, **b-** 80, **c-** 50 and **d-** 30 wt%PS latex annealed at 130  $^{\circ}$ C.

However, in the case of 30 wt%PS latex (Fig 6d) since the PS particles are diluted and completely imbedded in BuA1 matrix (Fig 6d), the hard latex nanospheres are well separated and completely coated with soft polymer, the contacts between small PS clusters was prevented. After annealing treatment at 150 °C (Fig 7), AFM images clearly shows the coalescence of PS particles for high PS content films (Fig 7a, b

and c). Whereas for 30 %wt PS, almost no connection between small dispersed PS clusters in BuA1 matrix contribute to latex film formation, only they remain as individual coalesced domains. Upon annealing the films at 200 °C, 100, 80 and 50 wt% PS content films (Fig 8a, b and c) show a more or less regular and continous surface structures depending on the PS content in the blend. However, despite the smooth surface for 30 wt%PS content blend film, surface morphology shows spherical domains which may be a sign for the spinodal decomposition process of this particular blend system [34,35].

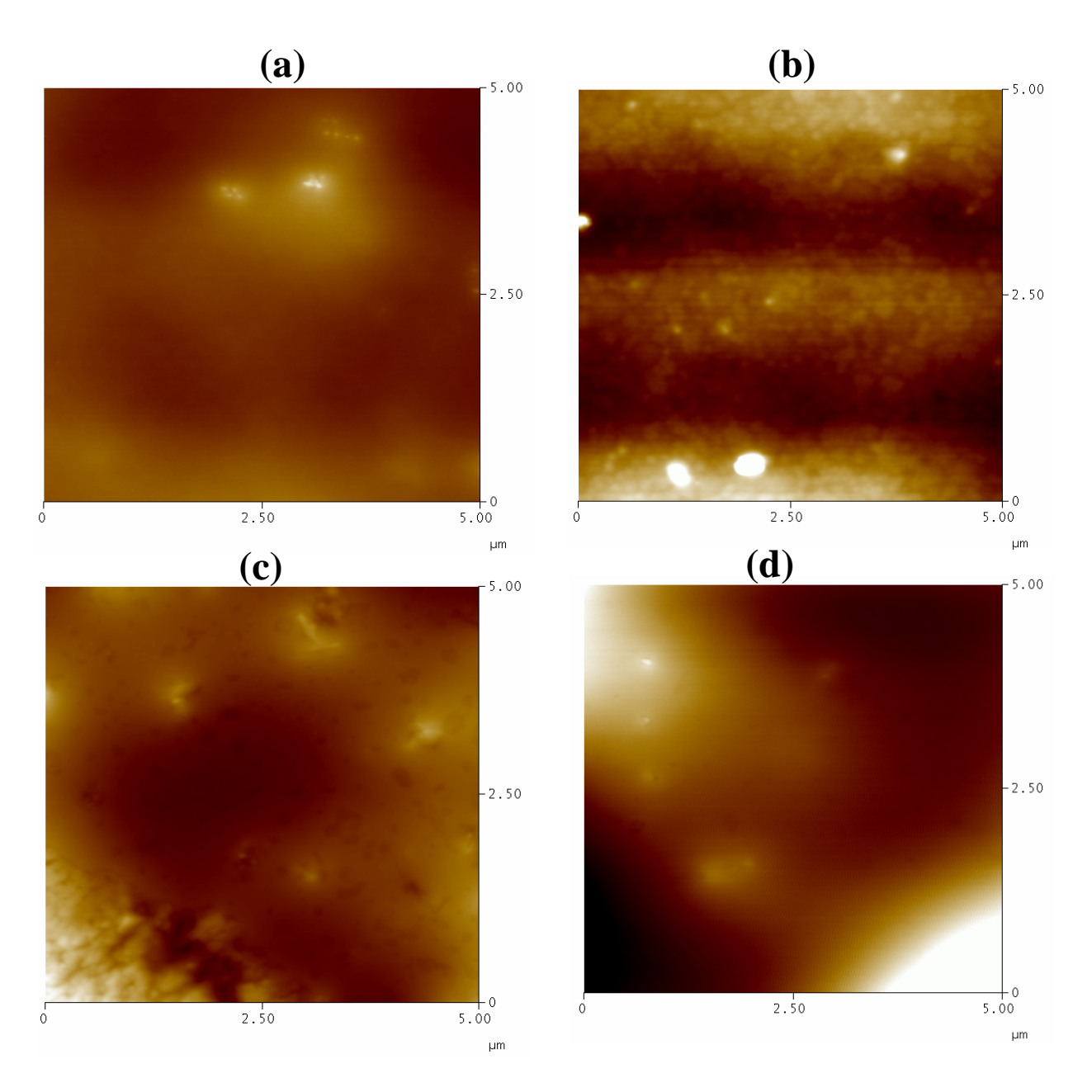


**Fig. 7.** AFM images of blend film prepared with **a-** 100, **b-** 80, **c-** 50 and **d-** 30 wt%PS latex annealed at 150  $^{\circ}$ C.

In order to see the evolution of transparency of the films depending on the blend composition, transmitted photon intensities, before annealing,  $(I_{tr})_i$  and after annealing,  $(I_{tr})_m$  at 200  $^{\circ}$ C from the blend films are plotted versus PS content in Fig 9

a and b, respectively. Before annealing (Fig 9a), films are quite transparent ( $I_{tr}$  up to 80%) at low latex content. As the hard latex content is increased ,  $I_{tr}$  decreases and become completely opaque ( $I_{tr}$  around 20%). As seen from the AFM pictures, when PS content increases the films containe a lot of voids (Fig 5a-c). However, for small PS content (Fig 5d), PS particles aggregated forming small dispersed clusters in BuA1 matrix.

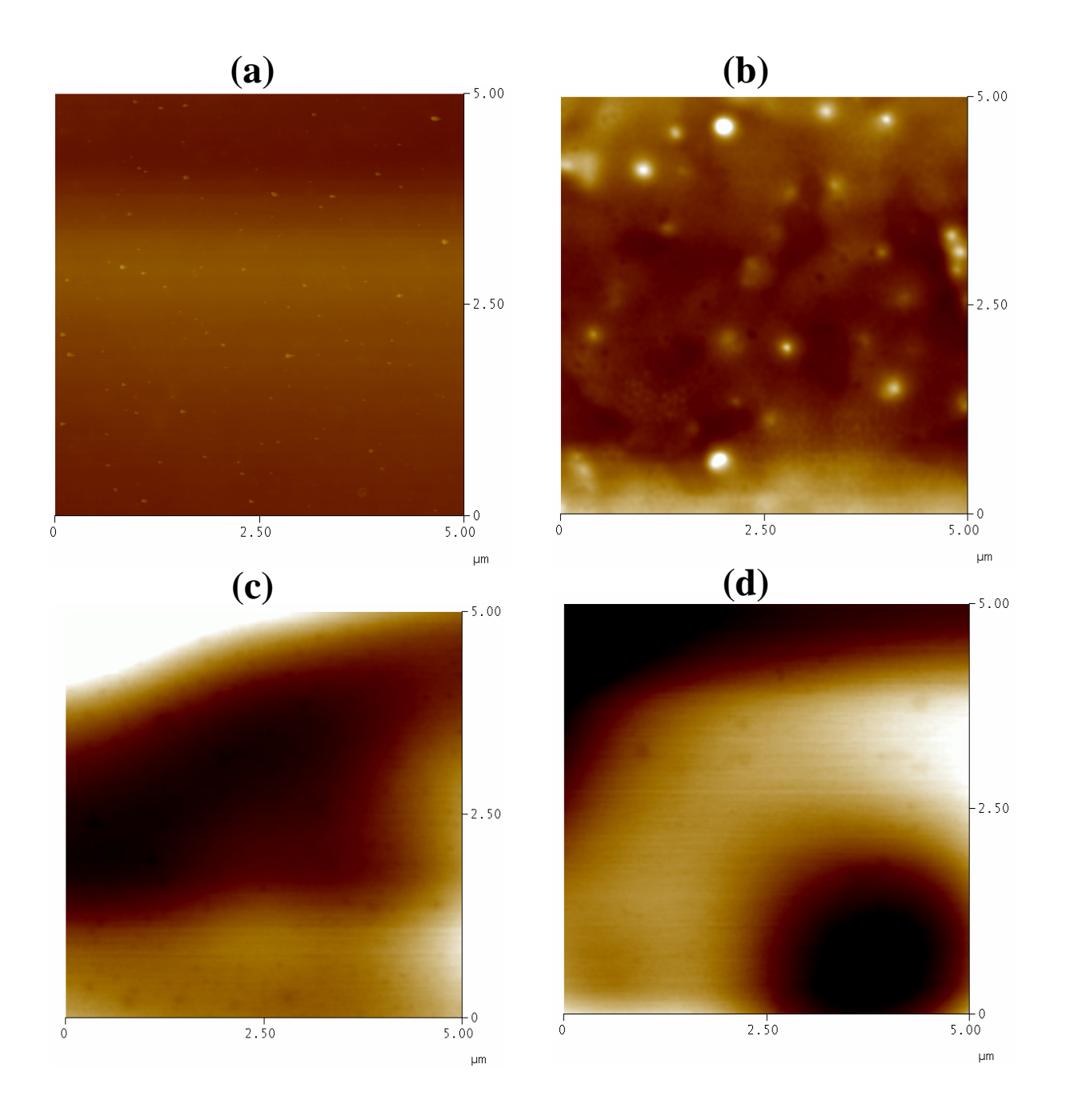


**Fig. 8.** AFM images of blend film prepared with **a-** 100, **b-** 80, **c-** 50 and **d-** 30 wt%PS latex annealed at 200  $^{\circ}$ C.

Despite the refractive indices of two polymers are somewhat different [36] (with differences of about 0.12), it is understood that the turbidity is mostly associated with aggregation [37] of hard latex and voids [9,10,17,21] in the film which can scatter the

light. However, after annealing at 200  $^{\circ}$ C three different regions are seen in Fig 10b. In region I and III, transparency of the films is high (up 60%) due to the continous film formation. The low transparency (around 40%) in region II is the result of the phase separation between PS and BuA1 due to the breakup and coarsening of the phase-separated domains.

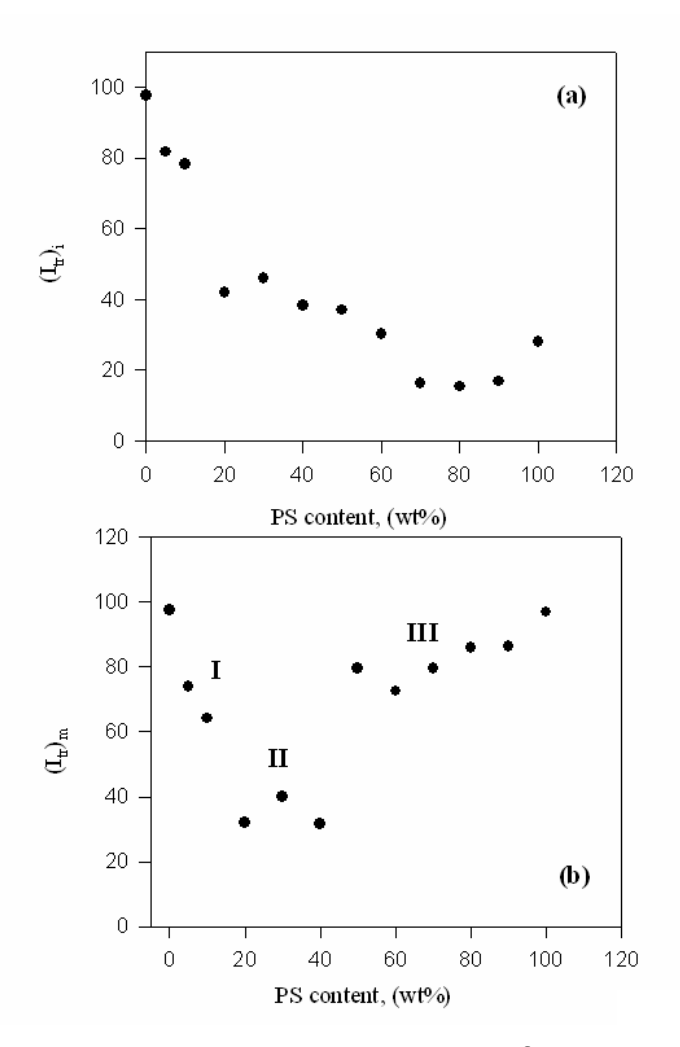


**Fig.9.** Plot of the transmitted light intensities, **a-** before annealing,  $(I_{tr})_i$  and **b-** after annealing at 200  ${}^{0}$ C,  $(I_{tr})_m$  versus PS latex content.

In this region the structure of the film is made of individual coalesced PS domains immersed in a continous matrix of BuA1 polymer. Since the size of PS domains are large with respect to the wavelenght of the visible light, they scatter the light which cause turbidity in the film [37]. Here it is interesting to note that transmittance of the blend films in region I and II does not change so much especially remains almost the same for region II before and after annealing. This shows that the clusters of PS particles before annealing remain as individual clusters imbedded in the BuA1-rich phase without coalescing with each other after annealing at 200  $^{\circ}$ C. Since the domain sizes in region I are smaller than those in region II, the transparency is higher in this region. On the other hand, in region III it is seen that the transparency of the blend films are greatly improved (I<sub>tr</sub> up to 80%) after annealing due to the formation of a continous film.

The increase in  $I_{tr}$  and  $I_p$  intensities in the (50-100)%wt PS range can be explained by void closure and surface smooting with annealing. On the other hand, the increase in  $I_P$  above  $T_0$  presumbably corresponds to the void closure process up to the  $T_h$  point where the healing process takes place [9,10]. Decrease in  $I_P$  above  $T_h$  can be understood by interdiffusion between polymer chains. To understand these phenomena, the following mechanisms and their formulations are proposed.

#### Void Closure

Void closure kinetics can determine the activation energy for viscous flow during latex film formation. Mackenzie and Shuttleworth [12] modeled the void closure by viscous flow under the action of surface energy using the equation

$$\frac{dr}{dt} = -\frac{\gamma}{2\eta} \left( \frac{1}{\rho(r)} \right) \tag{1}$$

This equation assumes that, a spherical void of radius r shrinks as function of time. where  $\gamma$  is the surface energy at the air/polymer interface, t is time, and  $\rho(r)$  is the relative density. It has to be noted that here the surface energy causes a decrease in void size and the term  $\rho(r)$  varies with the microstructural characteristics of the material, such as the number of voids, the initial particle size and packing. Here,  $\rho(r)$  can be defined as a volume ratio of polymeric materials to voids, where as r goes to zero  $\rho(r)$  increases. However, for large r values  $\rho(r)$  decreases.  $\eta$  is the viscosity of surrounding medium and the temperature dependence of viscosity is given with the following relation [38]

$$\eta = A \exp(\Delta H / kT) \tag{2}$$

where  $\Delta H$  is the activation energy of viscous flow i.e. the amount of heat which must be given to one mole of material for creating the act of a jump during viscous flow. A is a constant and k is Boltzman's constant. When the Eq 1 is integrated it is usually assumed that viscosity is independent of time, the interparticle voids are spherical and in equal size and that the number of voids stays constant during film formation (i.e.  $\rho(r) \propto r^{-3}$ ), then the following relation can be written

$$t = \frac{2AC}{\gamma} \exp\left(\frac{\Delta H}{kT}\right) \left(\frac{1}{r^2} - \frac{1}{r_o^2}\right)$$
(3)

Here, C is a constant related to relative density  $\rho(r)$ . As we stated before, decrease in void size (r) causes an increase in both  $I_{tr}$  and  $I_{P}$ . Since the scattering intensity,  $I_{s}$  varies with volume squared ( $I_{s}\alpha v^{2}$ ) of the scattering object [39] then it can be assumed that  $I_{tr}$  and/or  $I_{P}$  (=I) is inversely proportional to the  $6^{th}$  power of void radius, r then Eq 3 can be written as

$$t = \frac{2AC}{\gamma} \exp\left(\frac{\Delta H}{kT}\right) (I^{1/3}) \tag{4}$$

Here,  ${\rm r_o}^{-2}$  is omitted from the relation since it is very small compared to  ${\rm r}^{-2}$  values after void closure processes is started. Eq 4 can be solved for  ${\rm l_{tr}}$  and  ${\rm l_P}$  to interpret the results in Fig 2 and 4 as

$$I(T) = S(t) \exp\left(-\frac{3\Delta H}{kT}\right) \tag{5}$$

where  $S(t)=(\gamma t/2AC)^3$ . For a given time the logarithmic form of Eq 5 can be written as follows

$$LnI(T) = LnS(t) - \left(\frac{3\Delta H}{kT}\right)$$
 (6)

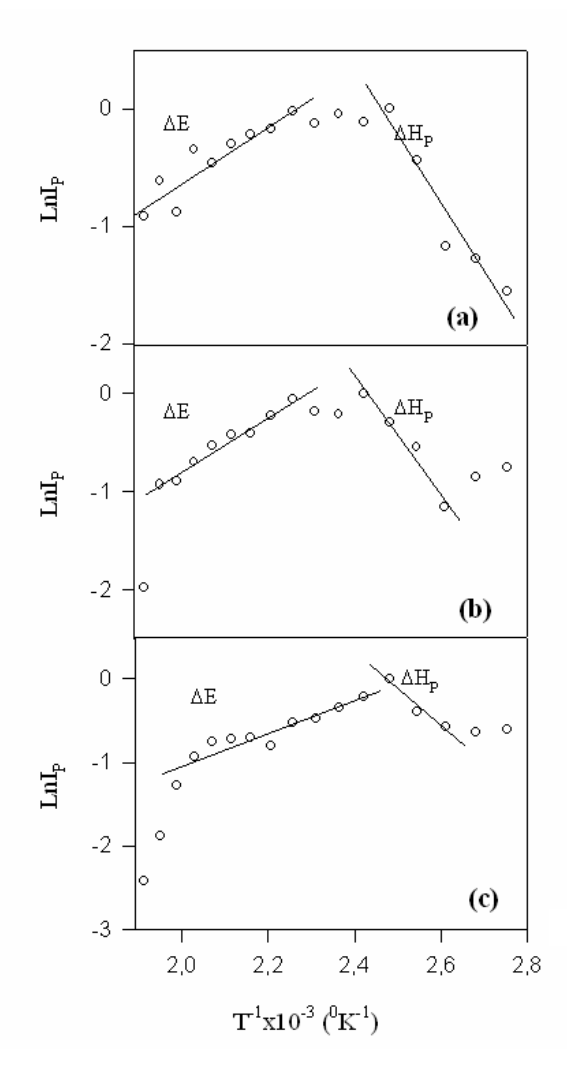


**Fig. 10.** The Ln(I<sub>P</sub>) versus T<sup>-1</sup> plots of the data in Fig 2a-c for the blend contain **a**-100, **b**-80 and **c**-50 wt%PS, respectively. The slope of the straight lines on right and left hand side of the graph produce  $\Delta H_P$  and  $\Delta E$  values, respectively.

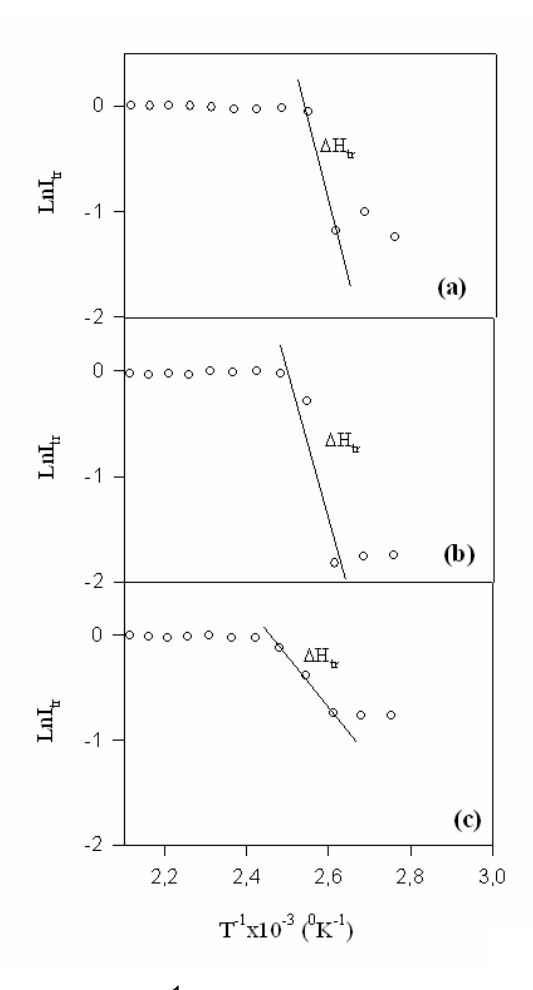


**Fig. 11.** The Ln( $I_{tr}$ ) versus T<sup>-1</sup> plots of the data in Fig 5a-c for the blend contain **a**-100, **b**-80 and **c**-50 wt%PS, respectively. The slope of the straight line produce  $\Delta H_{tr}$ .

As it is already argued above, the increase in both  $I_P$  and  $I_{tr}$  originate due to the void closure process, then Eq 6 was applied to  $I_{tr}$  and  $I_P$  below maxima for all film samples. Fig 10 and Fig 11 present the Ln $I_P$  and Ln $I_{tr}$  versus  $T^{-1}$  plots.  $\Delta H_P$  and  $\Delta H_{tr}$  activation energies were obtained by least squares fitting the data in Fig 10 and Fig 11 to Eq 6. The measured  $\Delta H_P$  and  $\Delta H_{tr}$  activation energies are listed in Table I where it is seen that activation energies do not change much i.e. the amount of heat which was required by one mole of polymeric material to accomplish a jump during viscous flow does not change by varying the blend composition in the films. Here it has to be noted that the measured activation energies for viscous flow were found to be different in different techniques, i.e.,  $\Delta H_P$  values were found to be smaller than  $\Delta H_{tr}$  values. Since pyrenes are labeled to the PS chain, one may argue that  $\Delta H_P$  values are produced at molecular level in comparison to  $\Delta H_{tr}$  values, which are produced using a macroscopic treatment, it is believed that  $\Delta H_P$  values are more reliable and can be trusted.

# Healing and Interdiffusion

The decrease in  $I_P$  was already explained in previous section, by interdiffusion of polymer chains. As the annealing temperature is increased above maxima, some part of the polymer chains may cross the junction surface and particle boundaries disappear, as a result  $I_P$  decreases due to transparency of the film. In order to quantify these results, the Prager-Tirrell (PT) model [40,41] for the chain crossing density can be employed. These authors used de Gennes's "reptation" model to explain configurational relaxation at the polymer-polymer junction where each polymer chain is considered to be confined to a tube in which executes a random back and forth motion[42]. The total "crossing density"  $\sigma(t)$  (chains per unit area) at junction surface then was calculated from the contributions  $\sigma_1(t)$  due to chains still retaining some portion of their initial tubes, plus a remainder  $\sigma_2(t)$  i. e. contribution comes from chains which have relaxed at least once. In terms of reduced time  $\tau = 2 w / N^2$  the total crossing density can be written as [40]

$$\sigma(\tau)/\sigma(\infty) = 2\pi^{-1/2}\tau^{1/2} \tag{7}$$

where v and N are the diffusion coefficient and number of freely jointed segment of polymer chain [40].

In order to compare our results with the crossing density of the PT model, the temperature dependence of  $\sigma(\tau)/\sigma(\infty)$  can be modeled by taking into account the following Arrhenius relation for the linear diffusion coefficient

$$v = v_o \exp(-\Delta E / kT) \tag{8}$$

Here  $\Delta E$  is defined as the activation energy for backbone motion depending on the temperature interval. Combining Eq 7 and Eq 8 a useful relation is obtained as

$$\sigma(\tau)/\sigma(\infty) = R_o \exp(-\Delta E/2kT)$$
(9)

where  $R_o = (8 \nu_o t/\pi N^2)^{1/2}$  is a temperature independent coefficient. The decrease in I<sub>P</sub> in Fig 3a-c above T<sub>h</sub> is already related to the disappearance of particle-particle interface. As annealing temperature increased, more chains relaxed across the junction surface and as a result the crossing density increases. Now, it can be assumed that I<sub>P</sub> is inversely proportional to the crossing density  $\sigma(T)$  and then the phenomenological equation can be written as

$$I_P(\infty) = R_0^{-1} \exp(\Delta E / 2k_B T) \tag{10}$$

Tab. I. Experimentally Produced Activation Energies.

PS content (wt%)	∆H <sub>P</sub> (kcal.mol <sup>-1</sup> )	ΔH <sub>tr</sub> (kcal.mol⁻ ¹)	ΔE (kcal.mol⁻ ¹)
50	2.91	3.18	7.77
60	3.23	7.93	6.36
70	4.51	7.42	4.45
80	3.93	9.25	11.23
90	7.14	8.21	4.28
100	3.58	11.18	9.55
average	4.22	7.86	8.77

Logarithmic plots of  $I_P$  vs  $T^{-1}$  are presented in Fig 10a, b and c for the films contain 100, 80 and 50 wt% PS content, respectively. The activation energy of backbone motion,  $\Delta E$  is produced by fitting the data in Fig 10 to Eq 10 and are listed in Table I. Here, we have to mention that though the fitting seems much nicer for pure PS film in Fig 10a, the fits in Fig 10b and c are not well behaved, i.e., the model is probably not well suited to the data due to the phase separation process between PS and BuA1 phases in these films.  $\Delta E$  value does not change with increasing PS content indicating that blend composition does not affect the backbone motion of the polymer chains across the junction surfaces. In addition,  $\Delta E$  values are slightly larger than the void closure activation energies. This result is understandable because a single chain needs more energy to execute diffusion across the polymer-polymer interface than to be accomplished by the viscous flow process.

# **Conclusions**

This study showed that the combined use of (UVV) and (SSF) investigation methods allows to understand the mechanisms of film formation from blends of hard and soft latex particles. For the 50-100%wt PS content film, two different film formation stages were observed upon annealing. In these films it was seen that annealing first lead to a complete closure of void between PS particles and forming very large PS domains. Coalescence of PS particles follows closely the completion of void closure and interdiffusion of PS chains sets up continous film. It was also seen that energies required for void closure and interdiffusion processes in these films do not change with varying the blend composition. However, no film formation stages were seen for the blend films if PS content is below 50%wt. UV results showed that below this fraction of PS, films exhibit phase separation. The AFM results are in excellent agreement with the results we determined via SSF and UVV.

## **Experimental**

#### Materials

## -Preparation of Latex Dispersions

The hard latex samples are composed of pyrene (P) labeled polystyrene (PS). These labelled latex was prepared via surfactant free radical emulsion polymerization in batch process. The polymerization was conducted in 50 ml reactor using; ionized

water (50ml), distilled styrene (5 g, total amount, 99% pure from Janssen), 1-Pyrenylmethyl methacrylate, (0.014 g) (PolyFluo<sup>TM</sup> 394 from Polyscince, Inc.) was used as such, and water soluble radical initiator potassium persulfate (KPS) (0.2 g) was used as received. The fluorescent monomer was solublized in 1 g styrene and KPS was dissolved in 3ml water before use. The polymerization was conducted under 300 RPM agitation, nitrogen atmosphere at 90°C during one hour and then at 70°C during 16 hours. These particles have a  $T_q$ =105  $^{0}$ C.

The soft latex samples are composed of Poly(n-butyl acrylate) (BuA1). These latex samples were prepared by semicontinuous process [33]. All reagents were from Merck (Darmstadt, Germany). Monomers: n-butyl acrylate (BuA) and acrylic acid (AA) were purified by filtration through basic alumina powder. The surfactant, sodium dodecyl sulfate (SDS) (purity over 99%), and initiator, ammonium persulfate ((NH<sub>4</sub>)<sub>2</sub>S<sub>2</sub>O<sub>8</sub>) (purity 99%), were used directly from the bottle. Distilled water was used throughout. The latex syntheses were performed in a double-wall 1.5-liter glass reactor, under a nitrogen blanket. The reaction temperature was adjusted to 75  $^{\circ}$ C for 3h and then to 82  $^{\circ}$ C for 2h. The synthesized core-shell latice is composed of BuA (99 wt%) and a small percentage of acrylate acid (1 wt%)[33]. They are fairly monodisperse, having all very similar mean diameters (97 nm) and has a T<sub>g</sub>(=-41  $^{\circ}$ C) below room temperature. Furthermore, the acrylic acid is well incorporated and a large majority of it is located in the particle shell [33].

# -Latex film preparation from blends

Latex blends were prepared by mixing known weights of the two latexes (PS and BuA1). Twelve different composition of blends with increasing (0, 5, 10, 20, 30, 40, 50, 60, 70, 80, 90 and 100) wt% of PS were prepared. These latex mixtures were mixed for several minutes to let the dispersion be sufficiently mixed. The mixed dispersion was then coated on a glass plate with the size of 2.5x0.8 cm² by placing the same number of drops and dried at room temperature. Then samples were separately annealed above  $T_g$  of PS for 10 min at temperatures ranging from 90 to 250  $^{\circ}$ C. The temperature was maintained within ±2  $^{\circ}$ C during annealing. After annealing, films were removed from the oven and cooled to room temperature.

#### Methods

## -Fluorescence measurements

After annealing, each sample was placed in the solid surface accesory of a Hitachi F-4010 Fluorescence Spectrometer. P was excited at 345 nm and fluorescence emission spectra were deteched between 360-500 nm. All measurements were carried out in the front-face position at room temperature. Slit widths were kept at 5 nm during all SSF measurements.

#### -Photon transmission Measurements

Photon transmission experiments were carried out using model UV-2101PC Shimadzu UV-Visible (UVV) scanning spectrometer. The transmittances of the films were recorded at 500 nm to see the evolution of transparency of the film samples. A glass plate was used as a standard for all UVV experiments and measurements were carried out at room temperature after each annealing process.

# -Atomic Force Microscopy (AFM) Measurements

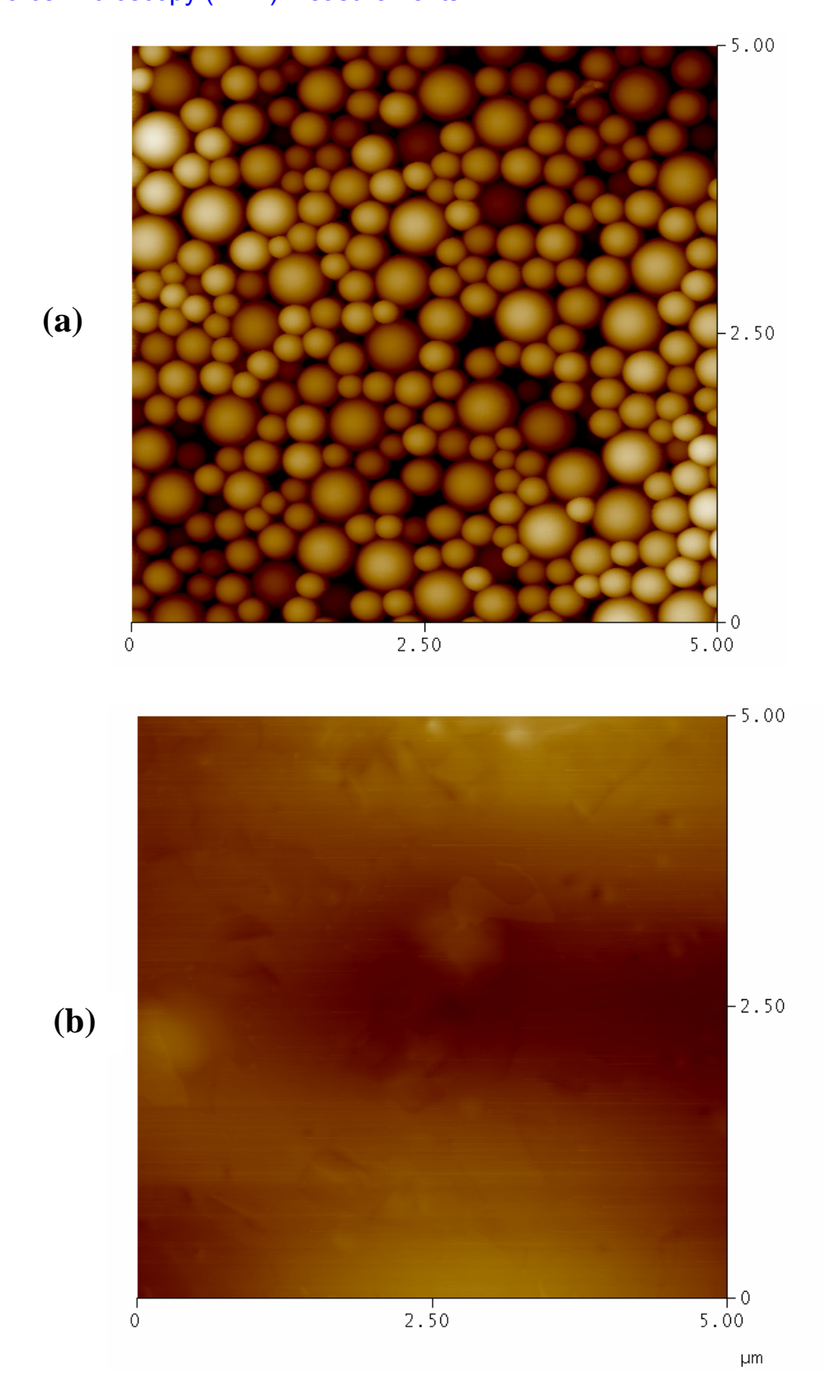


**Fig. 12.** Atomic Force Microscopy (AFM) images of PS/(BuA/MMA4) blend films with **a-** pure PS and **b-** pure BuA1 film before annealing.

Micrographs of the blend films were recorded with a NanoScope (R) IIIa multimode scanning probe atomic force microscope (AFM). The scan range was chosen between  $5\mu mx5\mu m$  to achieve a high resolution. Fig 12a and b show AFM images of individual latex components before annealing. The particles in the pure PS latex film (Fig 12a) are spherical and polydisperse. Here, the dark regions in the films corresponds to the unoccupied spaces (voids). AFM image of pure BuA1 film (Fig 12b) reveals an overall flat and smooth film surface. These particles are film forming at room temperature and form continous and void-free films.

# **Acknowledgements**

We would like to thank Mr. C. Contal who performed the AFM experiments and Dr. P. Marie for his help during my stay at ICS.

#### References

- [1] Provder Th., Winnik M. A., Urban M., Eds. Film Formation in Waterborne Coatings, ACS Symp. Ser., **1996**, 648.
- [2] Keddie J. L., Mater. Sci. Eng. 1997, R21, 101.
- [3] Mazur S. "Coalescence of Polymer Particles", Polymer Powder Processing, Ed. N. Rosenweig, John Wiley and Sons (1995).
- [4] Kim K. D., Sperling L. H. and Klein A., Macromolecules 1993, 26, 4624.
- [5] Pekcan Ö., Winnik M. A. and Croucher M. D., Macromolecules 1990,23, 2673.
- [6] Wang Y. and Winnik M. A., J. Phys. Chem. 1993, 97, 2507.
- [7a] Canpolat M. and Pekcan Ö., Polymer **1995**, 36, 2025, b. Canpolat M. and Pekcan Ö., Polymer **1997**, 38, 2595.
- [8] Pekcan Ö. and Arda E., Colloids Suf. A 1999, 153, 537.
- [9] Uğur Ş., Elaissari A. and Pekcan Ö., J. Coll. Int. Sci. 2003, 263, 674.
- [10a] Uğur Ş., Elaissari A. and Pekcan Ö., J. Coat. Technol. Res. **2004**, 1 (4), 305-313, b. Uğur Ş., Elaissari A. and Pekcan Ö., Polym. Adv. Technol. **2005**, 16, 405-412.
- [11a] Uğur Ş. and Pekcan Ö., Coll. Polym. Sci. **2005**, 284, 309-316, b. Uğur Ş. and Pekcan Ö., Phase Trans. **2005**, 78, No:7-8, 593-606.
- [12] Sperry P. R., Synder B. S., O'Dowd M. L., Lesko P. M., Langmuir **1994**, 10, 2619.
- [13] Mackenzie J. K., Shuttleworth R., Proc. Phys. Soc. **1949**, 62 (12-B), 838.
- [14] Vanderhoff J. W., Br. Polym. J. **1970**, 2, 161.
- [15] Yoo J. N., Sperling L. H., Glinka C. J., Klein A., Macromolecules 1991, 24, 2868.
- [16] Pekcan Ö., Trends Polym. Sci. **1994**, 2, 236.
- [17] Winnik M. A., Feng J. R., J. Coating Technol. 1996, 68, 39.
- [18] Eckersly S. T., Helmer B. J., J. Coat. Technol. 1997, 69 (864), 97.
- [19] Colombini D., Ljungberg N., Hassender H., Karlsson O. J., Polymer **2005**, 46, 1295
- [20] Feng J. F., Winnik M. A., Shivers RR and Clubb B., Macromolecules **1995**, 28, 7671-7682.
- [21] Keddie JL., Meredith P., Jones RAL and Donald AM, Langmuir 1996, 12, 3793.
- [22] Y. Cvevalier., Hidalgo M., Cavaille J. Y., Cabane B., Macromolecules **1999**, 32, 7887.
- [23] Miles IS, Multicomponent Polymer Systems, Burnt Mill: Harlow, (1992).
- [24] Winnik MA, Weng J., J. Coating. Technol. **1996**, 66, 99.

- [25] Paul D. R., Newman S., Polymer Blends; Academic Pres, New York **1978**, vol 1-2.
- [26] Butt H. J., Kuropka R., J. Coatings Tech. 1995, 67 (848), 101.
- [27] Patel A. A., Feng J., Winnik M. A., Vansco G. J., Dittman McBain C. B., Polymer **1996**, 37, 5577.
- [28] Feng J., Winnik MA, Siemiarczuk A., J. Polym. Sci. B: Polym. Phys. **1998**, 36,1115.
- [29] Pekcan Ö. and Arda E., J. Coll. Int. Sci. **2002**, 250, 471-477.
- [30] Canpolat M. and Pekcan O., Polymer 1995, 36, 4433.
- [31] Feng J., Pham H., Stoeva V., Winnik MA, J. Polym. Sci. B: Polym. Phys. **1998**, 36, 1129.
- [32] Uğur Ş. and Pekcan Ö., J. Coll. Int. Sci. 2004, 277, 359-365.
- [33] Belaroui F., Cabane B., Dorget M., Grohens Y., Marie P. And Holl Y., J. Coll. Int. Sci. **2003**, 262, 409.
- [34] Pollos I. S., Soliman M., Lee C. , Gido S. P., Rohr K. S., and Winter H. H., Macromolecules **1997**, 30, 4470.
- [35] Kwel T. K., Nishi T., Roberts R. F., Macromolecules **1974,** 7, 667.
- [36] Bohn L., in polymer Handbook, 2nd ed. Brandup J. and Immergut E. H., Eds. 1975, Wiley-Interscience, New York,.
- [37] Rosen S. L., Polym. Eng. Sci. 1967, 7(2), 115.
- [38] Tager A., "Physical Chemistry of Polymers" 1978, MIR, Moscow.
- [39] Voyutskii S. S., Colloid Chemistry, MR Publisher, Moscow (1978).
- [40] Prager S., and Tirrell M., J. Chem. Phys. 1981, 75, 5194.
- [41] Wool R. P., Yuan B. L. and McGarel O. J., J. Polym. Eng. Sci. 1989, 29, 1340.
- [42] De Gennes P. G., J. Chem. Phys. 1982, 76, 3322.